SYNTHESIS, CHARACTERIZATION, APPLICATIONS AND COMPUTATIONAL STUDIES OF CA_4 HYDROGELS INCORPORATED WITH ZnO NANOPARTICLES [CA_4 - ZnO]

Princy Sowmya R.[1], Nikila S.[1], Harini S.[1], Kubaib Attar[2], Imran Predhanekar[2], and Guhanathan S.[1]

[1]Department of Chemistry, Muthurangam Government Arts College (Autonomous), (Affilated to Thiruvalluvar University, Serkadu, Vellore-632 115),
Vellore-632002.

[2]Department of Chemistry, Islamiah College (Autonomous), Vaniyambadi – 653 752, Tamil Nadu, India
(Affiliated to Thiruvalluvar University, Serkadu, Vellore-632 115), Tamil Nadu, India

*Corresponding author Email: sai_gugan@yahoo.com

Abstract

In this work, hydrogels (CA_4) were synthesized through esterification reaction using 2-furoic acid (FA), triethanolamine (TEA), and Citric acid (CA) subsequently incorporated with nano-ZnO particles to obtain [CA_4-ZnO] hydrogels. By evaluating the synthesized [CA_4-ZnO] nanocomposite hydrogels with UV, FTIR, ^{1}H NMR, ^{13}C NMR, TGA and SEM-EDX analytical methods. It confirmed that nano Zinc oxide were incorporated within the CA_4 network. Swelling behavior and the pH range from 2.0 to 11.0 were used to closely study the properties of hydrogels. As a result, neutral media (pH 7.0) shows the highest swelling percentage, rather then acidic and alkaline medium. Swelling equilibrium results enhance greatly with increase in nano ZnO concentration. Thermo gravimetric analysis (TGA) showed that the hydrogels of the [CA_4-ZnO] nanocomposite were thermally stable up to 300 ^{0}C. The Antibacterial studies were conducted with the gram positive bacteria like *Staphylococcus aureus, Bacillus subtilis,* and Gram negative bacteria namely *Klebsiella pneumonia, Escherichia coli* produces excellent results in inhibition

percentage. The antifungal study shows the lower zone of inhibition. The Cytotoxic study indicates good percentage in cell viability and the antioxidant analysis exhibits good zone of inhibition percentage. The optimized hydrogels docking studies revealing that the biological activity has been improved with inclusion of nano ZnO in the hydrogels. [CA_4-ZnO] nanocomposite hydrogels with the latter protein showed a stronger and more favorable binding to Clumping Factor A. The [CA_4-ZnO] nanocomposite hydrogels is capable of overcoming drug resistance and nano zinc oxide based hydrogels had respective anti-bacterial and wound healing properties. Thus, the hydrogels explored in the present study be beneficial for tissue engineering, wound healing, and other high-performance uses.

Keywords: Nanocomposite hydrogels, Swelling behavior, Antibacterial studies, Antioxidant analysis, Molecular docking, Clumping Factor A.

INTRODUCTION

Hydrogels are polymeric networks effective in capturing and retaining massive amount of water. They are polymeric materials that can enlarge and store a significant volume of water within their structure while remaining insoluble in water. Due to their high water level, hydrogels exhibit a high degree of flexibility, resembling to the natural tissues. The hydrogels absorb water because of hydrophilic groups in the polymer backbone [1]. Hydrogels are characterized by their swelling capacity within the hydrogel network. However, polymer–water interaction forces are the primary factor responsible for hydrogel swelling. Polymer–water interactions, electrostatic forces, and osmotic pressure play the role in the expansion of hydrogel polymeric network. The swelling behavior of hydrogels can be categorized into non-ionic, ionic (anionic, cationic, and amphoteric), and hydrophilic hydrogels containing hydrophobic groups. The non-ionic hydrogels, like poly(N-vinyl pyrrolidone) and poly(ethylene oxide), swells in aqueous media because of water–polymer

interactions. The hydrogels exhibit good transparency and can be easily modified. Hydrogels are ecologically friendly and self-healing [2], Timely distribution of medicines or nutrients [3Hydrogels have the ability to sense changes due to pH, temperature, or metabolite Concentration etc., [4,5]. Chemical crosslinking enhances the mechanical strength of the hydrogels [6]. This approach is extremely effective for the formation of *in situ* hydrogels structures. Physical cross-linking techniques involve ionic interactions as well as temperature-dependent and pH-dependent mechanisms for cross-linking. [7]. The wide range of applications are tissue engineering and the design of biological tissues in both in vitro and in vivo systems [8,9], efficient wound therapy [10], drug delivery [11], gene therapy [12], wide range of tissue engineering applications, notably the repair of blood arteries, the skin, heart valves, cartilage, along with tendons [13], contact lens manufacturing [14], biosensorsand Waste water remediation technique [15]. Zinc oxide (ZnO) nanoparticles have attracted considerable attention in biomedical applications due to their excellent antibacterial activity, biocompatibility, and stability. ZnO nanoparticles can effectively inhibit the growth of a wide range of microorganisms through the generation of reactive oxygen species and the disruption of bacterial cell membranes. In addition to their antimicrobial properties, ZnO nanoparticles also promote wound healing by enhancing cell proliferation and tissue regeneration. Several metal and metal oxide nanoparticles, such as silver (Ag_2O) [16], gold (Au), copper oxide (CuO)[17] , titanium dioxide (TiO_2), Magnesium oxide (MgO) and zinc oxide (ZnO) [18], have been widely investigated for antibacterial and wound healing applications because of their strong antimicrobial efficiency and ability to accelerate the healing process. Therefore, ZnO nanoparticles were incorporated into the CA_4 matrix to prepare the CA_4–ZnO nanocomposite in order to improve its antibacterial performance and wound healing potential.

Bio-polymeric three-dimensional hydrogels networks are formed from biocompatible components that can absorb and hold large quantity of water while maintaining its structural integrity. Due to its biocompatibility, biodegradability, and tunable physicochemical characteristics, they have gained significant attention in biomedical applications. In the present study, the hydrogel network was developed using citric acid, triethanolamine, and 2-furoic acid as functional building components. Citric acid acts as an effective crosslinking agent due to the presence of multiple carboxylic groups, which facilitate the synthesis of a stable polymeric network through esterification and hydrogen-bonding interactions. Triethanolamine contributes to the stabilization of the hydrogel structure through intermolecular interactions, while 2-furoic acid introduces additional functional groups that enhance the physicochemical properties of the hydrogel.

To further improve the functional performance of the hydrogel, zinc oxide (ZnO) nanoparticles were incorporated into the polymeric matrix to form a CA_4–ZnO nanocomposite hydrogel. The incorporation of ZnO nanoparticles into the hydrogel network enhances its antimicrobial efficiency and promotes tissue regeneration, which is suitable for the biomedical applications.

2. EXPERIMENTAL

2.1 Methods

2.1.1 Stage I: Synthesis of Pre-polymers

The Citric acid (CA) was used as the monomer. A quantity of 0.025 mol (4.803 g) Citric acid (CA), were diluted in 5 mL of ethanol and then transferred in to the round-bottomed flask fitted with the mechanical stirrer until the monomer completely dissolved in ethanol.

Triethanolamine (TEA) [0.025 mol (3.3006 g)] diluted in 5 mL of ethanol was added to citric acid, drop by drop using a dropping funnel. The mixture had been stirred for an hour at 140 °C. The development of a sticky white gel implies the formation of pre-polymer (Citric acid-Triethanolamine [CT]).

2.1.2 Stage II: Synthesis of Bio-polymeric Hydrogels

2-Furoic acid (FA) (0.025 mol, or 2.802 g) were dissolved in 5 mL of ethanol and transferred into the pre-polyester CT and stirred continuously for 2 hours in mechanical stirrer up to 140 °C. The formation of glassy brown gel of Citric acid-Triethanolamine-2 Furoic acid (CTF) confirms the synthesis of parent hydrogels. The resultant gel was immersed in pure ethanol for 24 hours to eliminate unreacted monomers, further it was dried using a vacuum oven at 35 ^{o}C temperatures for 24 hours. A similar approach has been taken by altering the chemical composition of monomers. **Table 1** lists the experimental details of a series of synthesized biopolymeric hydrogels. Among the different series of hydrogels, CA_4 is taken for further research based on their higher swelling behavior compared with other series of synthesized hydrogels.

Table 1: Formulation of CA-TEA-FA in distinct composition

S.No	Samples	Monomer Composition (mole)			Description of Hydrogels
		CA	TEA	FA	
1	CTF	0.025	0.025	0.025	Transparent in nature -Brown glassy gel - Insoluble in water
2	FA_1	0.025	0.025	**0.01**	
3	FA_2	0.025	0.025	**0.02**	
4	FA_3	0.025	0.025	**0.03**	
5	FA_4	0.025	0.025	**0.04**	
6	TEA_1	0.025	**0.01**	0.025	
7	TEA_2	0.025	**0.02**	0.025	
8	TEA_3	0.025	**0.03**	0.025	
9	TEA_4	0.025	**0.04**	0.025	
10	CA_1	**0.01**	0.025	0.025	
11	CA_2	**0.02**	0.025	0.025	
12	CA_3	**0.03**	0.025	0.025	
13	CA_4	**0.04**	0.025	0.025	

2.1.3 Incorporation of Zinc oxide (ZnO) nanoparticles in CA_4 Biopolymeric Hydrogels

The 0.5 wt% of Zinc oxide (ZnO) nanoparticles with the particle size of less than 100 nm were incorporated into the CA_4 biopolymeric hydrogel matrix and stirred constantly for 1 hour at 35 ^oC, leading to the formation of nanocomposite biopolymeric hydrogels [CA_4-ZnO]. Similarly, 1.0 wt% and 2.0 wt% of ZnO was carried out in same process with CA_4 biopolymeric hydrogels, separately as shown in **Table 2**.. The ZnO concentrations (0.5, 1.0 and 2.0 wt %) were calculated based on the total weight of the synthesized polymer hydrogels matrix. The samples were named CA_4Z_1, CA_4Z_2, and CA_4Z_3 based on the CA_4 hydrogel matrix composition and the ZnO nanoparticles. Here, CA_4 represents the base hydrogel formulation (0.040 + 0.025 + 0.025 moles), **Z** indicates ZnO nanoparticles, whereas the subscript numbers i.e., 1, 2 and 3 correspond to 0.5 wt%, 1.0 wt% and 2.0 wt% of ZnO nanoparticles, respectively.

Table 2: Formulation of CA_4 Hydrogel in distinct composition with ZnO nanoparticles

S.No	Sample	CA_4 Hydrogel Composition (moles)	ZnO Nanocomposite (wt %)	Description of Hydrogels
1	CA_4Z_1	**0.040** + 0.025 + 0.025	**0.5**	Transparent in nature - Brown glassy gel - Insoluble in water
2	CA_4Z_2	**0.040** + 0.025 + 0.025	**1.0**	
3	CA_4Z_3	**0.040** + 0.025 + 0.025	**2.0**	

2.2 CHARACTERIZATIONS

2.2.1. Fourier transform infrared (FTIR) spectroscopy analysis

The FTIR Shimadzu 8400S spectrophotometer was utilized to successfully examine the molecular structure of [CA_4-ZnO], utilizing samples made with the standard KBr disc method. The spectra were obtained between 4000 to 500 cm^{-1}.

2.2.2 UV–Vis Spectrophotometer

An ultraviolet-visible double-beam (UV-Vis) spectrophotometer was used to characterize the [CA_4-ZnO] complex. Periodically, samples of the compound were taken in order to track the reaction's conclusion. The sample spectra were captured between 190 to 1100 nm in wavelength.

2.2.3 Scanning Electron Microscopy (SEM -EDX)

To evaluate the polymer and cross linker concentrations affect surface shape, we studied the hydrogel [CA_4-ZnO] using advanced scanning electron microscopy (SEM). This SEM, combined with an Energy-Dispersive X-ray spectrometer (EDX), facilitates rapid and exact qualitative and quantitative study of elemental compositions, offering crucial insights of our investigation.

2.2.4 High-Resolution Transmission Electron Microscopy (HR-TEM)

200–300 kV for High-Resolution Transmission Electron Microscopy (HR-TEM) is an advanced characterization technique that uses a high-energy electron beam to obtain ultra-high-resolution images and structural information of materials at the nanoscale.

2.2.5 Thermo gravimetric analysis (TGA)

Thermo gravimetric analysis (TGA) with SDT Q 600, Polymeric hydrogels thermal characteristics was investigated using simultaneous TGA (TA Instruments). TGA curves were captured at temperatures ranging from ambient to 500 ° C.

2.2.6 Swelling behavior

The 0.200 g of dried hydrogel was soaked in buffer solutions ranging in pH from 2.0 to 11.0 in room temperature. In regular time intervals, the expanded hydrogels was carefully withdrawn from the swelling medium, and then wiped with the filter paper to remove excess water, weighed, and then returned to the original solution. This rigorous approach guarantees that their absorption capacity is measured. Finally, surface water from the hydrogels was removed with filter paper. The efficiency of water consumption can be calculated using the following equation (1):

$$S_{eq}\% = \frac{W_{Sq} - W_I}{W_I} \times 100$$

Where, W_I= Initial weight of the dried out hydrogel

W_{Sq}= The weight of the enlarged sample at equilibrium.

2.3 Biological Applications

2.3.1 Antibacterial studies

The antibacterial study was investigated by conventional agar well diffusion method. Each bacterial isolate was immersed in Brain Heart Infusion (BHI) broth and diluted around 10^5 colony-forming units (CFU) per milliliter. They were flood-inoculated onto the surface of Media (Mueller Hinton Agar for Bacteria) and dried. Using the sterile cork borer, the wells of 5 mm were made in the agar medium. Subsequently, 30 µL of the sample solution (50µg compound dissolved in 500

μL DMSO) was placed in each well. The plates were then incubated for 18 hours at 37°C for bacterial cultures. Antimicrobial activity was determined by measuring the diameter of the inhibition zone. Dimethyl Sulfoxide (DMSO) was employed as the solvent control while ciprofloxacin was utilized as the standard antibacterial agent. The tests were performed in triplicate. The hydrogels were induced with bacteria specifically *Staphylococcus aureus, Bacillus subtilis, Klebsiella pneumonia*, and *Escherichia coli*.

2.3.2 Antifungal studies

The Antifungal activity is carried out with *C.albicans* and *A.niger*. The Clotrimazole 20 mg/well is taken as standard. The diameter of the zone of inhibition (mm) was taken as the indicator of activity against the test pathogens.

2.3.3 Cytotoxic studies

The mouse fibroblast cell line (L929) was plated separately on a 96-well plate at a concentration of 1×104 cells/well in DMEM (Dulbecco's Modified Eagle Medium)media containing 10% fetal bovine serum and 1X antibiotic antimycotic solution in a CO_2 incubator set at 37˚C with 5% CO_2. After being cleaned with 1X PBS (Phosphate-Buffered Saline) in 200 μL , the cells were cultured for 24 hours in serum-free medium with different concentrations of the test sample and DMSO (25%) as the positive control.. At the end of the treatment period, the medium was aspirated from the cells. MTT solution [0.5 mg/mL of (3-(4,5-dimethylthiazol-2-yl)-2,5-diphenyltetrazolium bromide)] prepared in 1X PBS was added, and the cell was incubated for 4 hours at 37˚C in a CO_2 incubator. After incubation period, the medium containing MTT was discarded and the cells were rinsed with 200 μL of PBS. The formed crystals were dissolved in100 μL of DMSO and mixed thoroughly. The color intensity development was assessed at 570 nm, and the development of

purple-blue formazan dye was evaluated by measuring the absorbance 570 nm through a microplate reader.

2.3.4 Antioxidant studies

Blois's (1958) approach was used to measure the sample's DPPH (2,2-diphenyl-1-picrylhydrazyl) radical scavenging activity. 0.5 ml of the sample solution in methanol was mixed with the 2.5 ml of a 0.5 mM methanolic DPPH solution. The reaction mixture was shaken well and kept in the dark at room temperature for 30 minutes. The absorbance at 517 nm was measured using UV spectrophotometer. Ascorbic acid was taken as the positive control. The percentage of the DPPH free radical scavenging was determine using the standard formula.

% of Inhibition = Absorbance of control – Absorbance of sample / Absorbance of control ×100.

2.3.5 Computational Studies

A pilot computational study was determined to investigate the antibacterial activity and protein binding aspects of CA_4 hydrogels and ZnO nanoparticles incorporated hydrogels. Therefore, the [CA_4–ZnO] nanocomposite hydrogels were subjected to molecular docking studies.

3. RESULTS AND DISCUSSION

3.1.1 FT-IR Spectroscopy of [CA_4 - ZnO] Nanocomposite Hydrogels

A stretching frequency observed at 3360 cm^{-1} relates to the hydrogen bonded O-H stretching vibration [19,20], which shows the decreasing of stretching frequency from 3414 cm^{-1} to 3360 cm^{-1}

might be due to the incorporation of nano ZnO into the polymer network. The peak at 2982 cm^{-1} represents the C-H stretching vibration. A distinct sharp peak at 1732 cm^{-1} ascribed to C= O stretching [21]. A new absorption peaks at 1610 cm^{-1} and 1474 cm^{-1} were attributed to the COO^- stretching vibrations. The prominent spectral peak at 1294 cm^{-1} is due to the presence of C-N stretching vibrations found in triethanolamine. The C-O stretching vibration was seen in 1176 cm^{-1} of the polyester network. The peak at 1073 cm^{-1} and 1041 cm^{-1} were due to C-O-C stretching frequency. The spectral peak appeared at 670 cm^{-1} which confirms the incorporation of zinc oxide nanoparticles in the main chain of hydrogels as shown in **Fig. 1** [22].

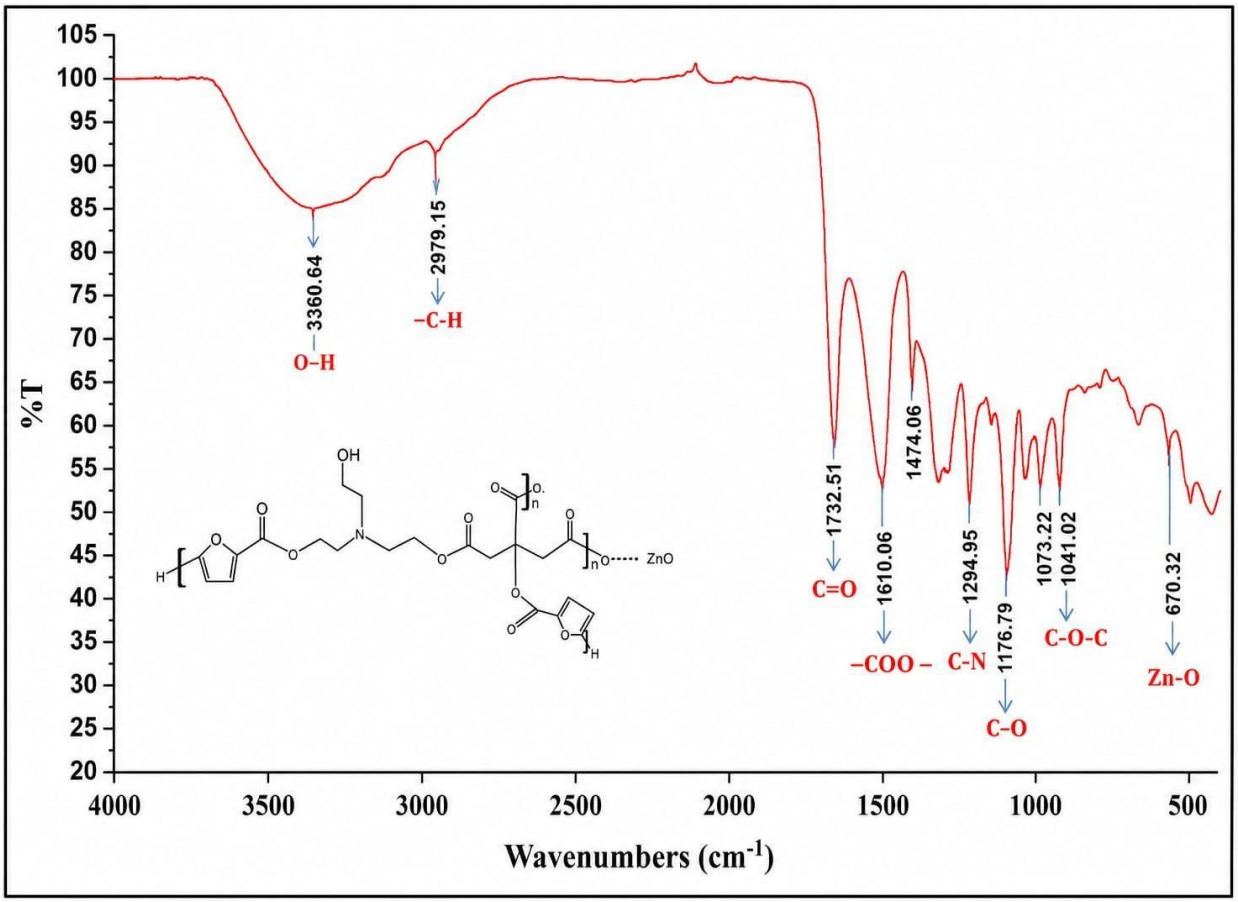

Fig.1: FT-IR Spectroscopy of [CA_4 - ZnO] Nanocomposite Hydrogels

3.1.2 UV Spectroscopy of [CA_4 - ZnO] Nanocomposite Hydrogels

UV-Visible spectroscopy is a key analytical technique used to characterize citric acid, 2-furoic acid, triethanolamine based hydrogels incorporating zinc oxide (ZnO) nanoparticles. This method helps to confirm the incorporation of ZnO nanoparticles in hydrogel matrix. **Fig. 2** clarifies the UV-visible spectral finding of [CA_4-ZnO] nanocomposite hydrogels. ZnO nanoparticles absorb ultra UV-visible light most effectively between 250 to 800 nm [23]. The wavelength spectrum of [CA_4 - ZnO] revealed a broad absorption peak at 300 nm, corresponding to absorbing capacities of 0.1 respectively. The absorbance of a nanocomposite hydrogel is caused by $n \rightarrow \pi^*$ transitions. The λmax primarily involving chromophores with a carbonyl group. This transition involves an electron from non-bonding (n) orbital, specifically a one-pair on a heteroatom like oxygen being promoted to an antibonding (n*) orbital.

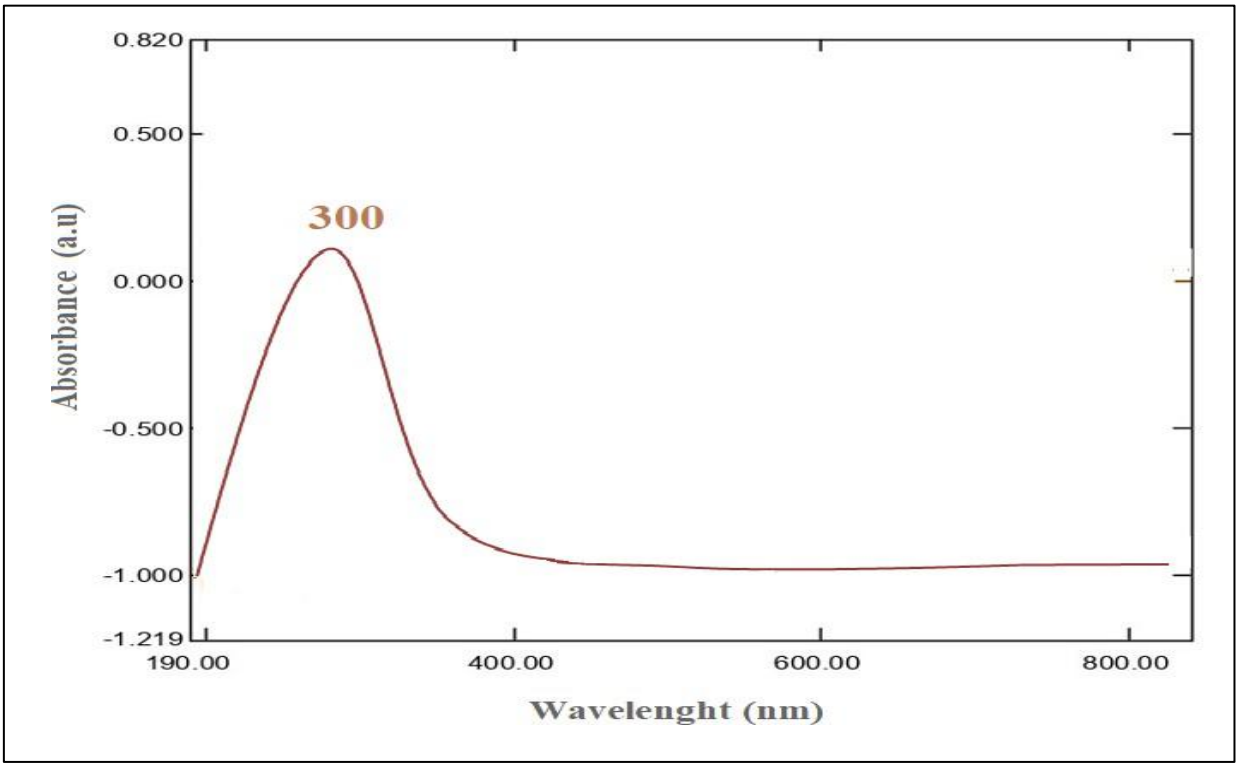

Fig.2: UV Spectroscopy of [CA_4 - ZnO] Nanocomposite Hydrogels

3.1.3 SEM & EDX analysis of [CA_4 - ZnO] Nanocomposite Hydrogels

The surface morphology of the synthesized [CA_4–ZnO] nanocomposite hydrogel was examined using the CA_4Z_3 sample by Scanning Electron Microscopy (SEM).The SEM image (**Fig.3)** shows a heterogeneous, non-porous, with rough surface structure due to hydrogel matrix packed with ZnO nanoparticles, which are scattered irregularly. The interaction of the hydrogel polymer chains with ZnO increases swelling ability, and functional qualities.

To validate the synthesis of the [CA_4 - ZnO] complex of CA_4Z_3 nanocomposite hydrogels, EDX analysis was performed, and the resulting peaks are shown in (**Fig.4)**. The EDX analysis shows that the produced nano composite contains ZnO NPs. In weight percentage, the respective amount of C, O, N, and Zn were 56.16, 30.69, 3.29 and 7.51 %, respectively. The plot of [CA_4 -

ZnO] nanocomposite hydrogels shows the presence of carbon, nitrogen, oxygen, and zinc (**Table 3**).

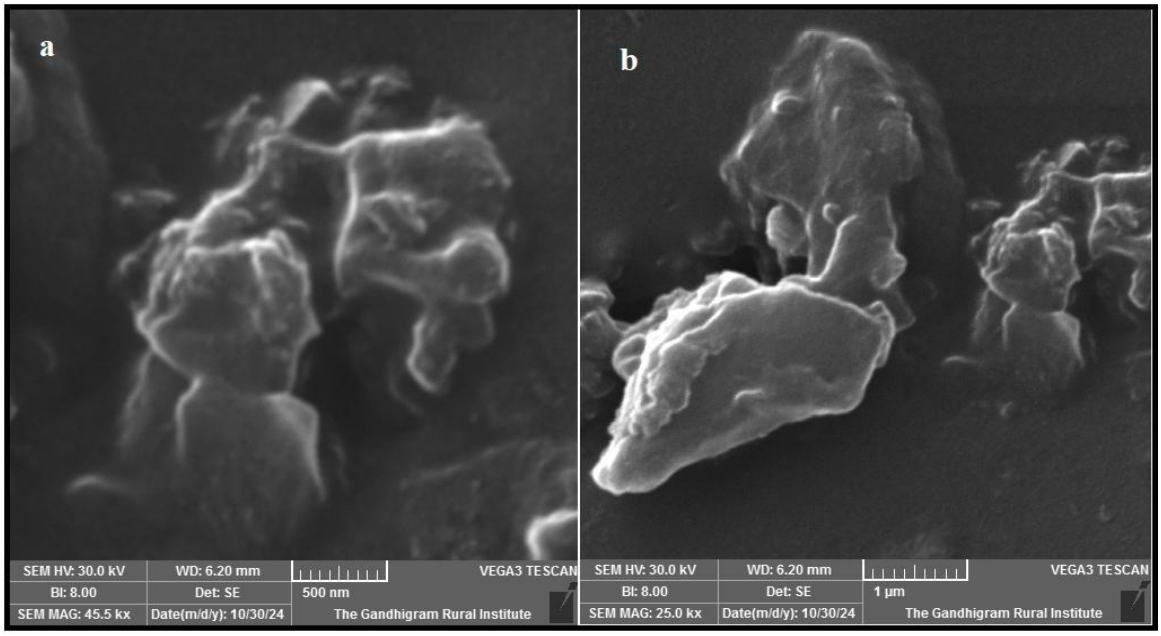

Fig.3 : SEM analysis of [CA_4 - ZnO] Nanocomposite Hydrogels of CA_4Z_3

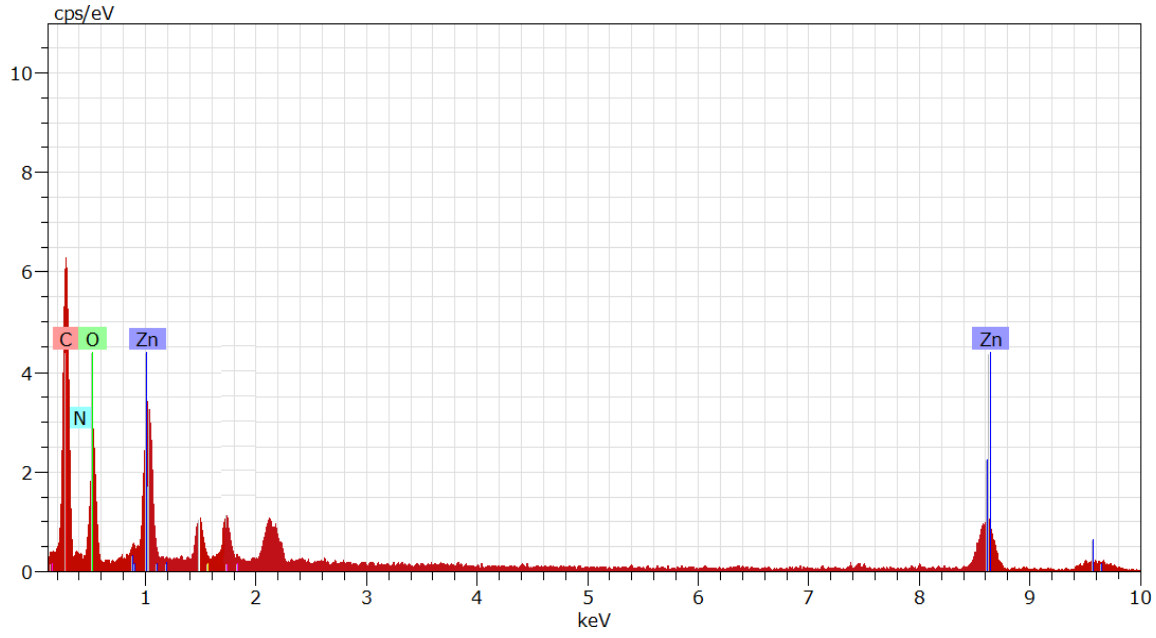

Fig. 4 : EDX analysis of [CA_4 - ZnO] Nanocomposite Hydrogels of CA_4Z_3

Table. 3: The weight percentage of elements in [CA_4 - ZnO] Nanocomposite Hydrogels of CA_4Z_3

Sl.No	Elements	Atomic number	Weight percentage
1	Carbon	6	56.16
2	Oxygen	8	30.69
3	Nitrogen	7	3.29
4	Zinc	30	7.51

3.1.4 HR-TEM analysis of [CA_4 - ZnO] Nanocomposite Hydrogels

The size and structure of nanoparticles within the hydrogel network are examined using transmission electron microscopy (TEM). TEM pictures shows the spherical ZnO NPs evenly scattered and located in the CA_4-ZnO hydrogel matrix. The usual size of CA_4-ZnO was 38 nm (**Fig. 5)**. The well-defined spherical morphology of the ZnO nanoparticles indicates strong interaction between hydrogel matrix and the ZnO nanoparticles. Furthermore, the lower concentrations of spherical ZnO nanoparticles increased biological activity as it is evident from antibacterial studies [24] .

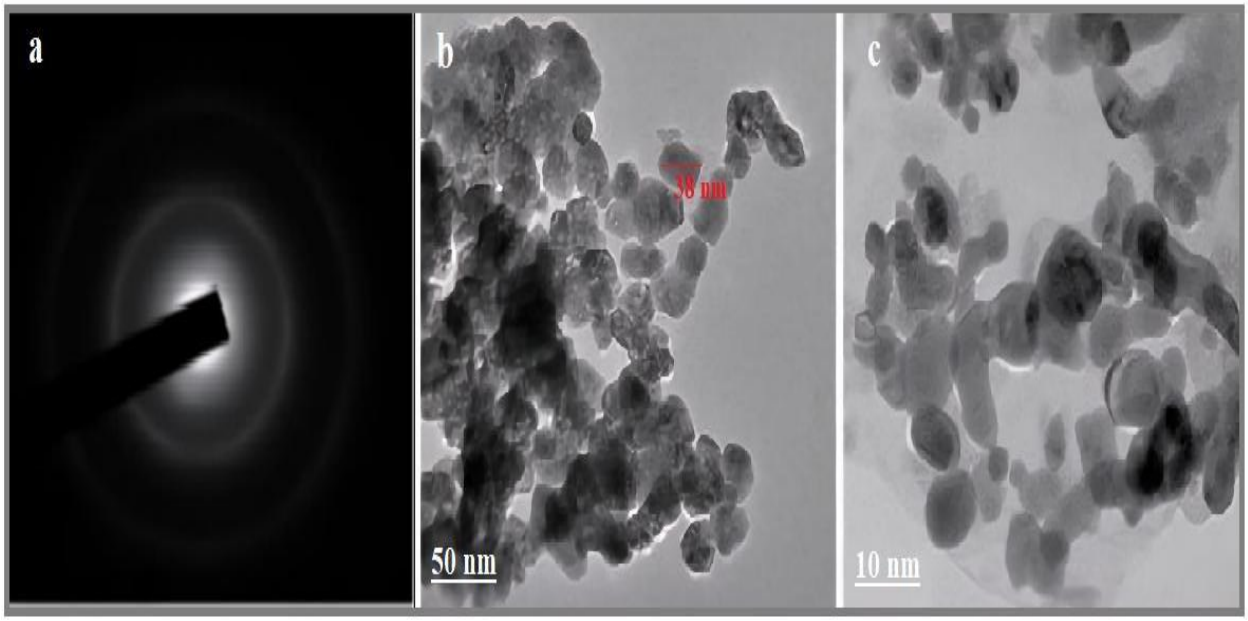

Fig. 5 : **HR-TEM analysis of [CA_4 - ZnO] Nanocomposite Hydrogels**

3.1.5 TGA of [CA_4 - ZnO] Nanocomposite Hydrogels

Thermogravimetric Analysis (TGA) was to study the thermal stability in [CA_4 - ZnO] nanocomposite hydrogel as shown in **Fig. 6**. The TGA curve shows three-stage disintegration. The earliest step of deterioration occurs between 50°C and 100°C, lead to 9 % drop in weight due to the elimination of residual water. The second stage decay occurred at temperatures ranging from 150 to 250 °C, which results in a 23% weight loss caused by the breakdown of the 2-furoic acid substitutes from the hydrogel material's (**Fig. 6**). The third step of degradation is seen at 300 °C, resulting in a 16 % weight loss because of the breakdown of ZnO nanoparticles embedded in the nano hydrogel network [25]. In conclusion, the TGA study reveals that the ZnO nanocomposite hydrogel has considerable thermal stability, with several degradation stages that include water loss, polymer decomposition etc,. In general ZnO nanoparticles exhibit higher thermal stability under normal conditions, but its stability is affected by factors like the presence of other materials impurities and high temperature environment, which can lead to decomposition, Hence in our case,

due to the interaction of biopolymeric hydrogels which found to be inferior due to polymeric filler interactions [26].

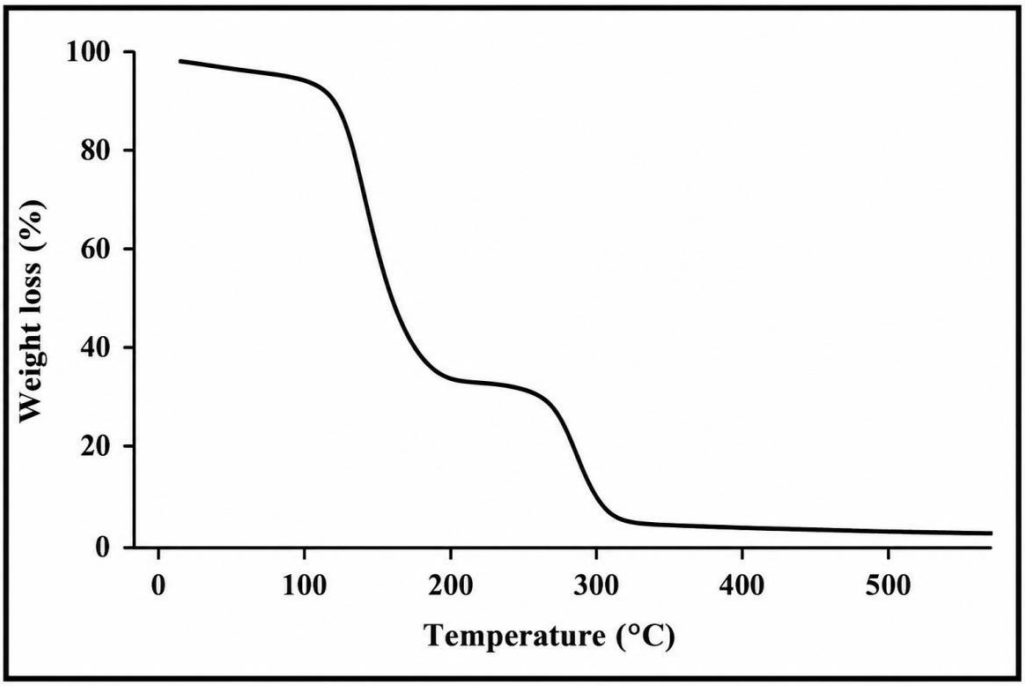

Fig. 6 : TGA of [CA_4 - ZnO] Nanocomposite Hydrogels

3.1.6 Swelling equilibrium (%) of [CA_4 - ZnO] Nanocomposite Hydrogels

The ZnO nanoparticles of 0.5 %, 1.0 % and 2.0 % namely CA_4Z_1, CA_4Z_2 and CA_4Z_3 were incorporated in CA_4 hydrogels.. The swelling behavior of CA_4-ZnO nanocomposite hydrogels at varies pH values (2.0, 4.0, 7.0, 9.0, and 11.0) and the results was shown in **Table 4**. As the swelling equilibrium values of the hydrogels have pH- dependent swelling, with maximal swelling observed at neutral to slightly alkaline (pH 7-9), owing to the ionization of functional groups (such as -COOH and -OH) in the polymeric matrix, which improves electrostatic repulsion and favors higher water uptake. CA_4Z_3 had the largest swelling percentage (127% at pH 7), followed by CA_4Z_2 (121%), and CA_4Z_1 (117%) as shown in **Fig 7**. Increasing the concentration of ZnO nanoparticles

appears to boost swelling capacity, could be due to interactions with hydrophilic groups. At acidic pH (2-4), swelling ratios were reduced due to functional group protonation, which resulted in hydrogen bonding and network contraction. At higher alkaline pH 11, swelling was partially reduced, resultant of charge shielding and partially breakdown of the hydrogel network [27]. Overall, the swelling investigation demonstrates that including ZnO nanoparticles into the hydrogel is advantageous for applications in drug administration, wound dressing, and biomedical systems that require controlled release at physiological pH [28]. The biological activities for the present investigation were carried out with CA_4Z_3 nanocomposite hydrogels due to their good swelling behavior.

Table. 4: Swelling equilibrium (%) studies of [CA_4 - ZnO] at different pH

S.No	Sample	CA_4 Synthesized Hydrogel (in grams)	ZnO Nano Particles (wt%)	Swelling Equilibrium (%) pH 2	pH 4	pH 7	pH 9.0	pH 11
1	CA_4Z_1	0.200	0. 5	100	107	118	104	100
2	CA_4Z_2	0.200	1.0	108	113	120	115	107
3	CA_4Z_3	0.200	2.0	**112**	**117**	**127**	**121**	**117**

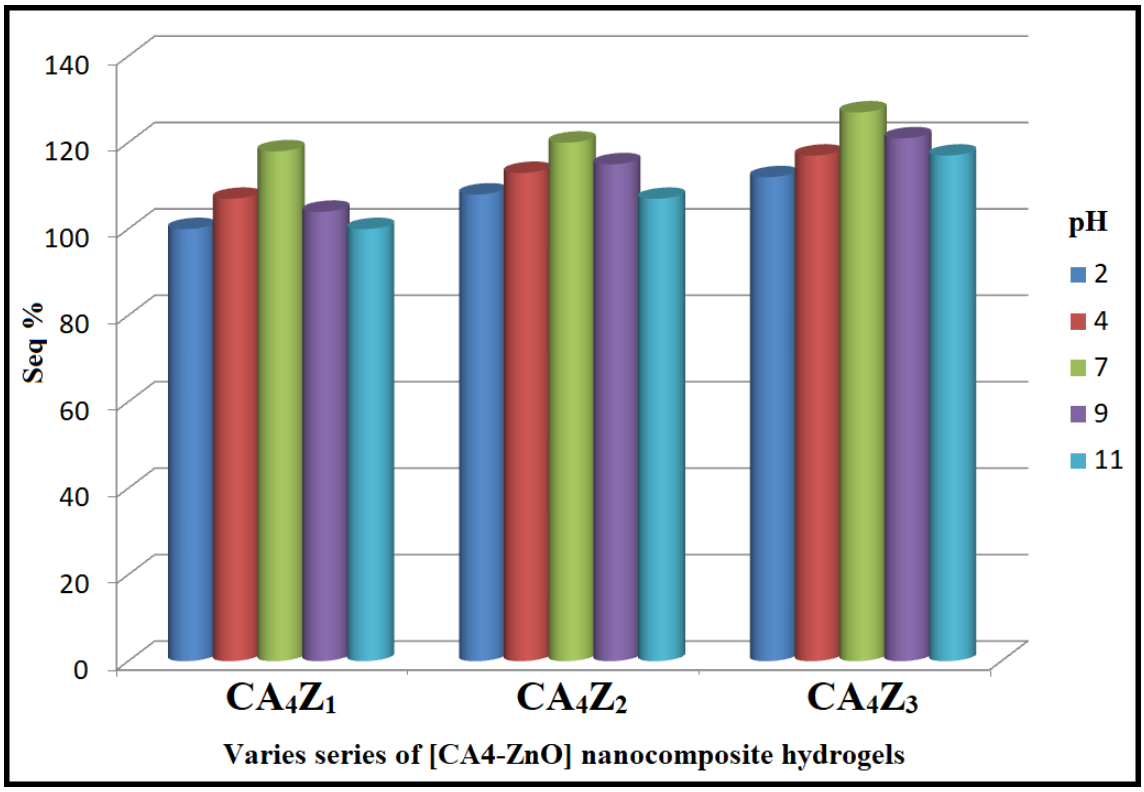

Fig. 7 : Graphical representation of Seq % studies of [CA_4 - ZnO] at different pH

3.2 Biological activity of [CA_4 - ZnO] Nanocomposite Hydrogels

3.2.1 Antibacterial activity

CA_4Z_3 outperformed all other [CA_4 - ZnO] hydrogel compositions in terms of antibacterial performance, as shown in **Fig 8**. The activity was studied towards gram positive (*S. aureus* and *B. subtilis*) and the gram negative (*E. coli,* and *K. pneumoniae*) strains of bacteria with Ciprofloxacin as the standard reference drug. Standard Ciprofloxacin inhibits pathogens that involve *S. aureus* (25 mm), *B. subtilis* (18 mm), *K. pneumonia* (20 mm), and *E. coli* (30 mm). The CA_4Z_3 hydrogels have inhibitory zones at 0 mm on *E. coli*, 8 mm in *S. aureus*, 10 mm in *B. subtilis*, and 6 mm on *K. pneumoniae* (**Fig. 8**). These observations and findings indicates that the hydrogel shows moderate inhibitory zone with the *S. aureus, B. subtilis* and *K. pneumonia*, where as *E. coli* shows no antibacterial activity owning to variations in their cell membrane permeability towards the

antibacterial agent [29]. As a result, these data show that CA_4Z_3 hydrogels have moderate inhibitory effects with the potential for biological applications.

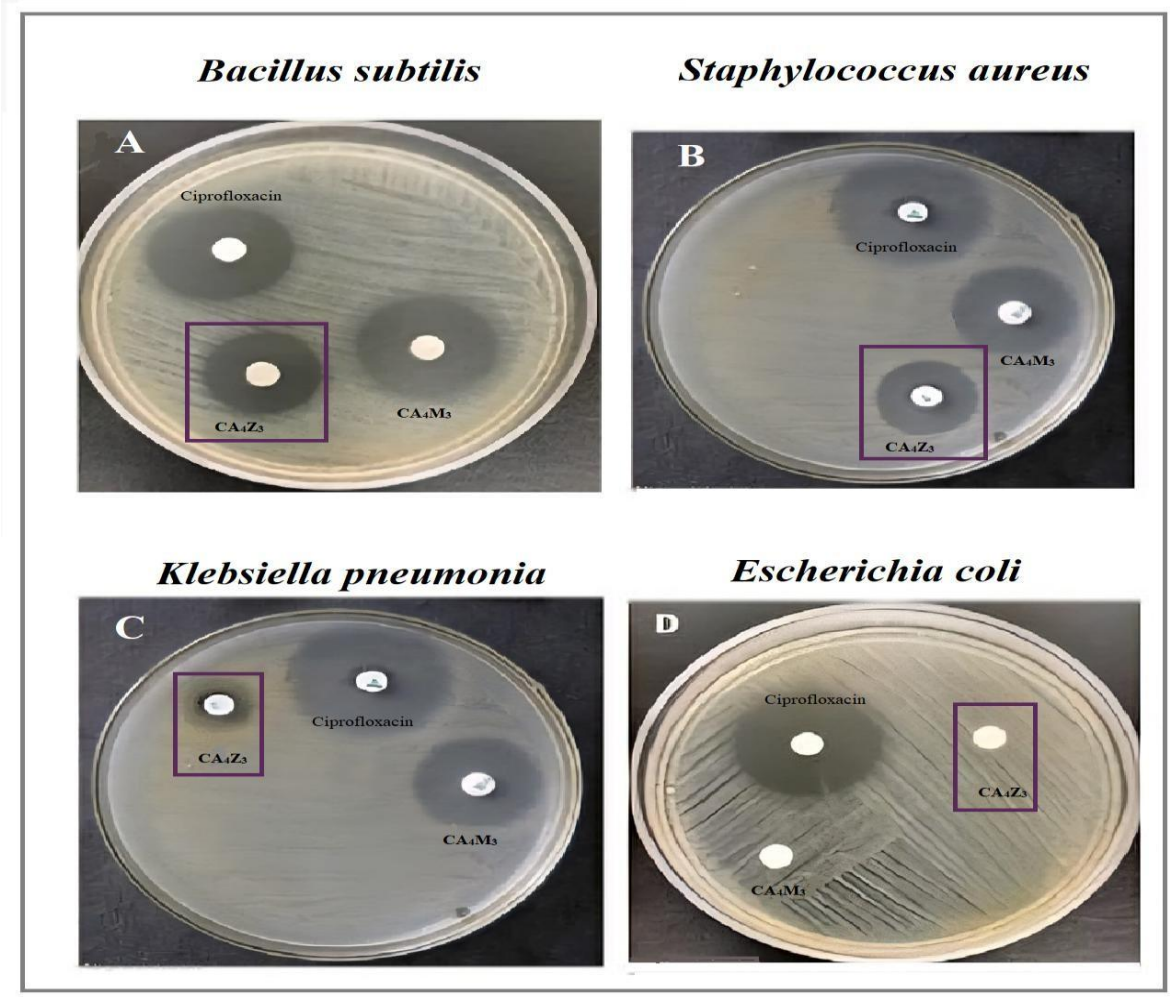

Fig. 8 : Antibacterial activity of CA_4Z_3 Nanocomposite Hydrogels

3.2.2 Antifungal activity

The hydrogels was evaluated towards the antifungal activity against the fungal strains like *Candida albicans* and *Aspergillus niger* using the agar well diffusion method. The standard antifungal drug Clotrimazole exhibited zones of inhibition of 16 mm in *Candida albicans* and 26 mm in *Aspergillus niger*. In comparison, the CA_4Z_3 hydrogel at a concentration of 300 mg/well

produced a 4 mm inhibition zone against *Candida albicans*, while no inhibition (0 mm) was observed against *Aspergillus niger* (**Fig.9**). These study reveals that the antifungal activity of the hydrogel is significantly lower than the standard drug. The limited inhibition may be attributed to the robust chitinous cell walls and melanin pigments present in these fungi, which enhance resistance to oxidative stress and reduce the susceptibility of the cells to ZnO nanoparticles attack [30]. Nevertheless, the incorporation of ZnO nanoparticles into polymeric hydrogel matrices may still provide a synergistic antifungal platform with potential applications in biomedical and agricultural fields.

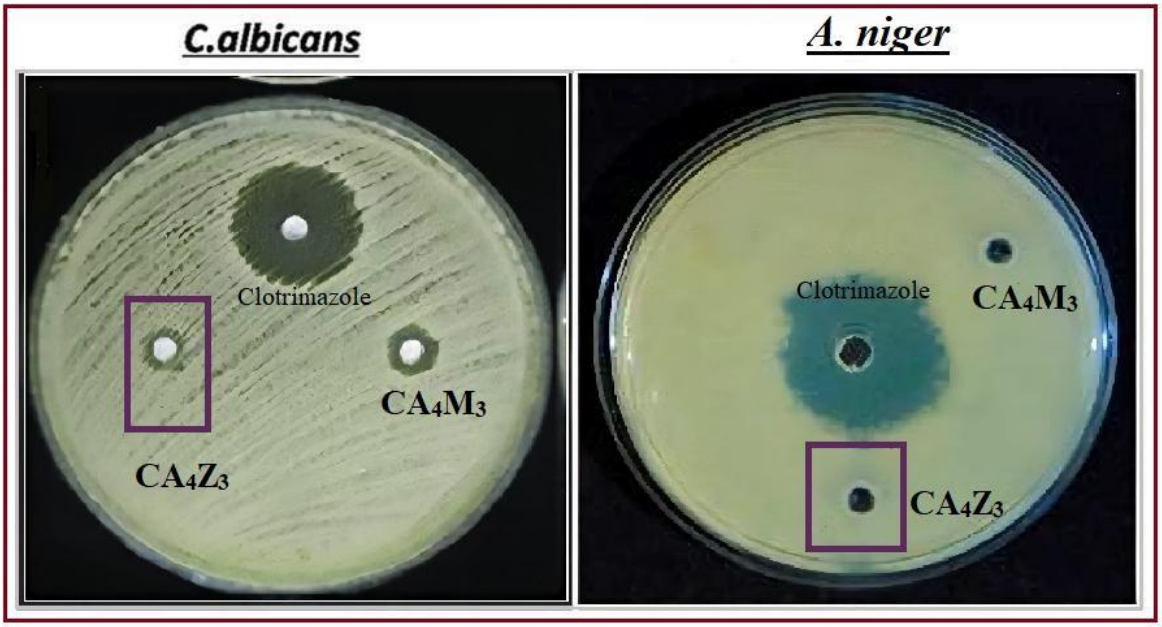

Fig. 9 : Antifungal activity of CA_4Z_3 Nanocomposite Hydrogels

3.2.3 Cytotoxicity activity

Several studies on the cytotoxicity investigated by MTT assay for ZnO nanoparticles have been conducted, with had an effect on a wide range of animal cells [31]. **Fig 10** shows the sustainability % of CA_4Z_3 nanocomposite hydrogels. The concentrations of 25, 50, 100, 250, and 500 µg/ml yielded percentages of 95, 90, 90, 85, and 82 % respectively. CA_4Z_3 is classified as non-

toxic as defined by ISO 10993-5 [32]. The average cell viability is greater than 80 % in all concentrations. As the result, among CA_4-ZnO nanocomposite hydrogels, CA_4Z_3 hydrogels exhibits good percentage of cell viability especially in case of low concentrations (25, 50, and 100 µg/ml) which is good and safe to use in biomedical applications (**Fig. 11**).

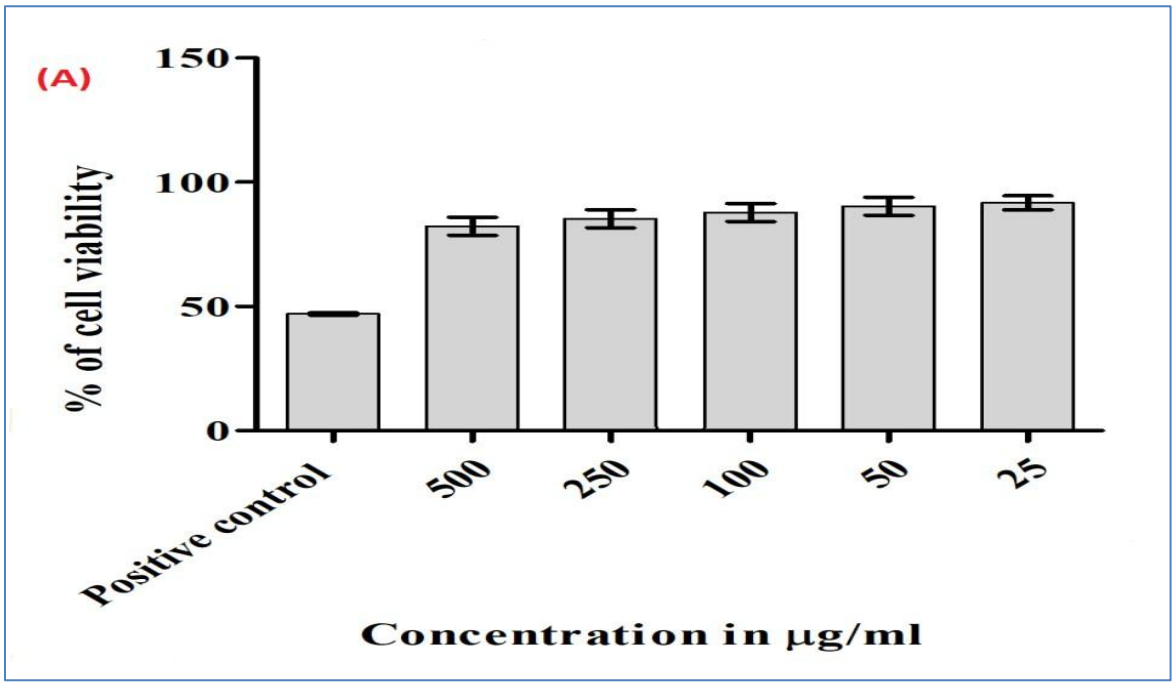

Fig. 10: MTT Assay of CA_4Z_3 at different concentrations

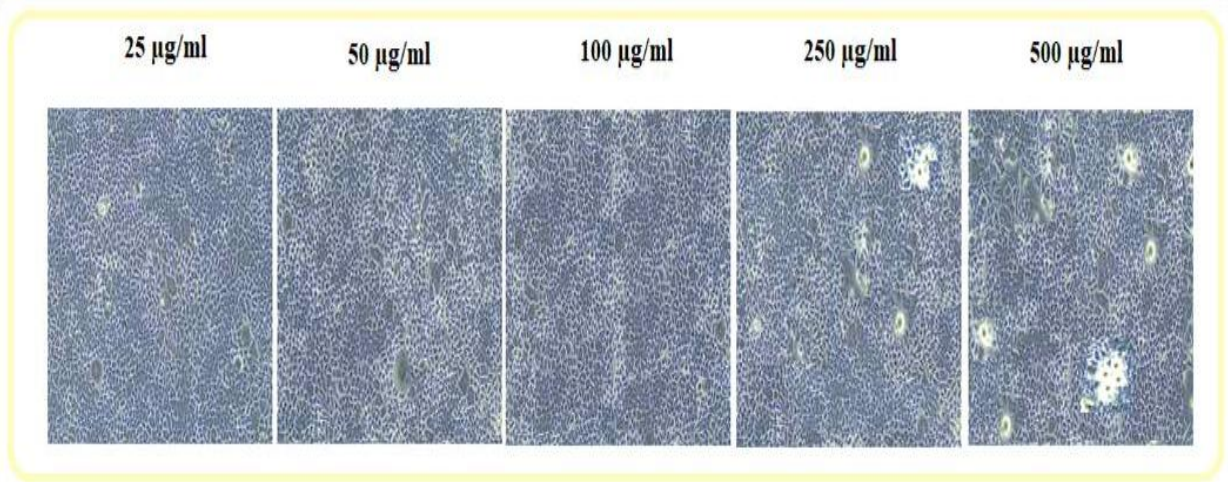

Fig. 11: The Cytotoxicity MTT assay of CA_4Z_3 at various concentrations

3.2.4 Antioxidant activity

The antioxidant activity of CA_4Z_3 nanocomposite hydrogels was measured with DPPH radical scavenging assay using Ascorbic acid as the reference, in which the inhibition rates range from 32%, 42%, 67%, 90%, and 94% across various concentrations (25, 50, 100, 250, and 500 µg/ml). CA_4Z_3 hydrogels had the highest antioxidant capability, inhibiting DPPH radicals at concentrations of 42%, 53%, 61%, 68%, and 79% (25, 50, 100, 250, and 500 µg/ml) as in **Fig. 12**.

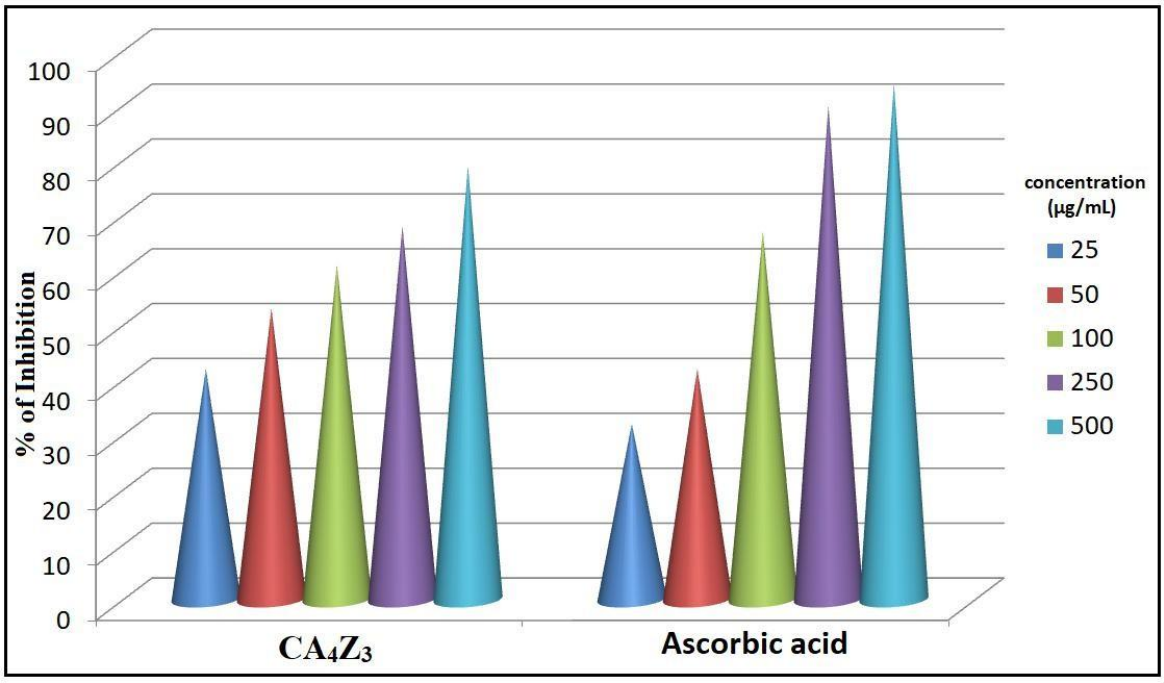

Fig. 12 : Antioxidant activity of CA_4Z_3 at distinct concentrations

At lower concentrations (25 and 50 µg/ml), CA_4Z_3 exhibits moderate inhibition, while ascorbic acid exhibits lesser inhibition. At medium concentrations (100-250 µg/ml), CA_4Z_3 activity slowly increases then the ascorbic acid. At the maximum dose (500 µg/ml), CA_4Z_3 shows good inhibition when compared to the ascorbic acid. The results suggest the resulting ZnO nanocomposite hydrogel exhibits significant antioxidant properties, that may be attributed to the

presence of the ZnO nanoparticles free radical interactions. It promotes the electron donation and the transfer of hydrogen to DPPH radicals in hydrophilic functional groups (-OH, -NH, -COOH) in the hydrogel matrix. The interaction within ZnO nanoparticles and their polymeric network facilitates more significant radical-scavenging efficacy. The IC_{50} of CA_4Z_3 was 149 µg/mL for DPPH method. The scavenging activity and IC_{50} value are opposite to each other[33]. The identical reports have also been found in literature according to Patel et al., 2011[34].

3.3 Computational Studies of CA_4-ZnO nanocomposite hydrogels

3.3.1 Density Functional Theory (DFT)

Since the CA_4–ZnO nanocomposite hydrogels showed biological activity, DFT and molecular docking studies was conducted to explore their mechanism of action. Initially an IRC (intrinsic reaction coordinate) analysis was carried out using three basic monomers namely citric acid, Triethanolamine and 2-Furoic acid which was utilized in the synthesis of the hydrogels. The IRC study revealed the structure selected for the optimization using the DFT level. The monomers was further optimized at the 6-31 D level with B3LYP (Becke, 3-parameter, Lee–Yang–Parr) and FMOs' (Frontier Molecular Orbital) were visualized to evaluate the MO (Molecular Orbital) aspects of reactivity. After achieving optimized geometry, the Molecular Electrostatic Potential (MESP) was generated to identify the probable regions of the molecule. The optimized molecule was used for docking studies. The values derived from the DFT calculations for the CA_4-ZnO nanocomposite hydrogels as shown in **Table 5**.

Table. 5: The values generated from DFT calculations of CA_4-ZnO nanocomposite hydrogels

Description	**HOMO** eV	**LUMO** eV	**Band gap** eV	**Energy** H	**Dipole** D	**Symmetry**
CA_4 - ZnO	-6.171	-2.086	4.085	-3740.41	7.8291	C1

The FMO analysis reveals that although the three monomers combine to form the hydrogel. The IRC results revealed that the FMOs spread unevenly across the monomers. But after the optimization it is seen that the HOMO (Highest Occupied Molecular Orbital) is centered on the Triethanolamine-part of the hydrogel and the LUMO (Lowest Unoccupied Molecular Orbital) spreads slightly over the Citric acid moiety very near to the ZnO nanoparticles in the hydrogels (**Fig 13**). The 2-Furoic acid part shows no lobes over its structure, indicates the lack of reactive space at its centre. Denser lobes near the ZnO nanoparticles part suggests that the transition metal complex has created enough lobes near its centre for reactivity. The MESP displays the distribution of electrostatic potential across the molecular surface, including some positive region as shown in **Fig 14 & Fig.15**. This suggests that this moiety helps to achieve the desired biological activity through electronic effects, owing both the negative and positive regions. A higher potential region was observed near the ZnO nanoparticles part and the biological activity is enhanced with inclusion of ZnO nanoparticles metal in the hydrogels.

FMO	**CA_4-ZnO**
HOMO	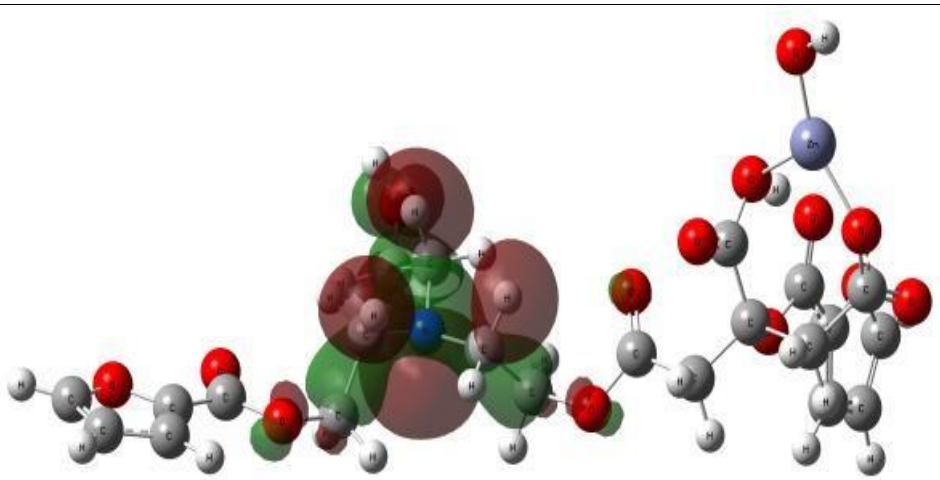
LUMO	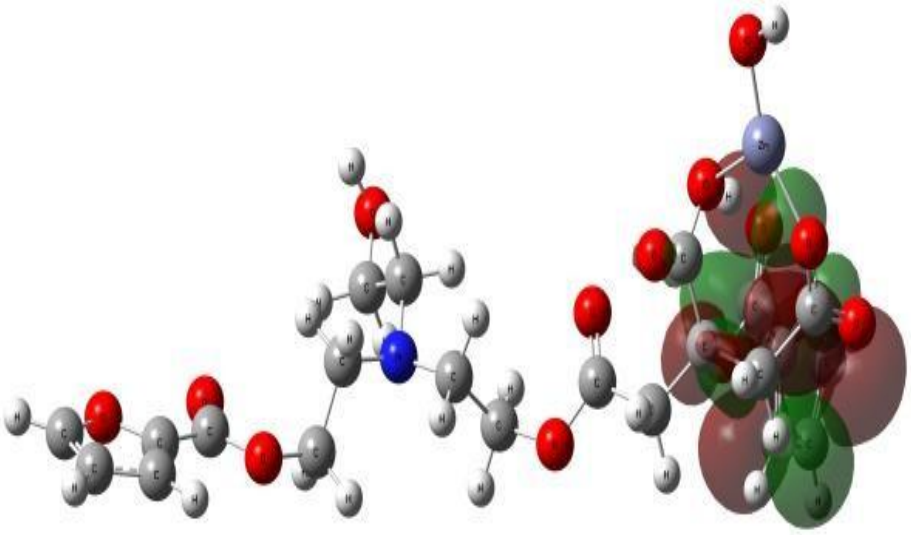

Fig. 13 : Fragment molecular orbital (FMO) and intrinsic reaction coordinate (IRC) of the CA_4-ZnO nanocomposite hydrogels

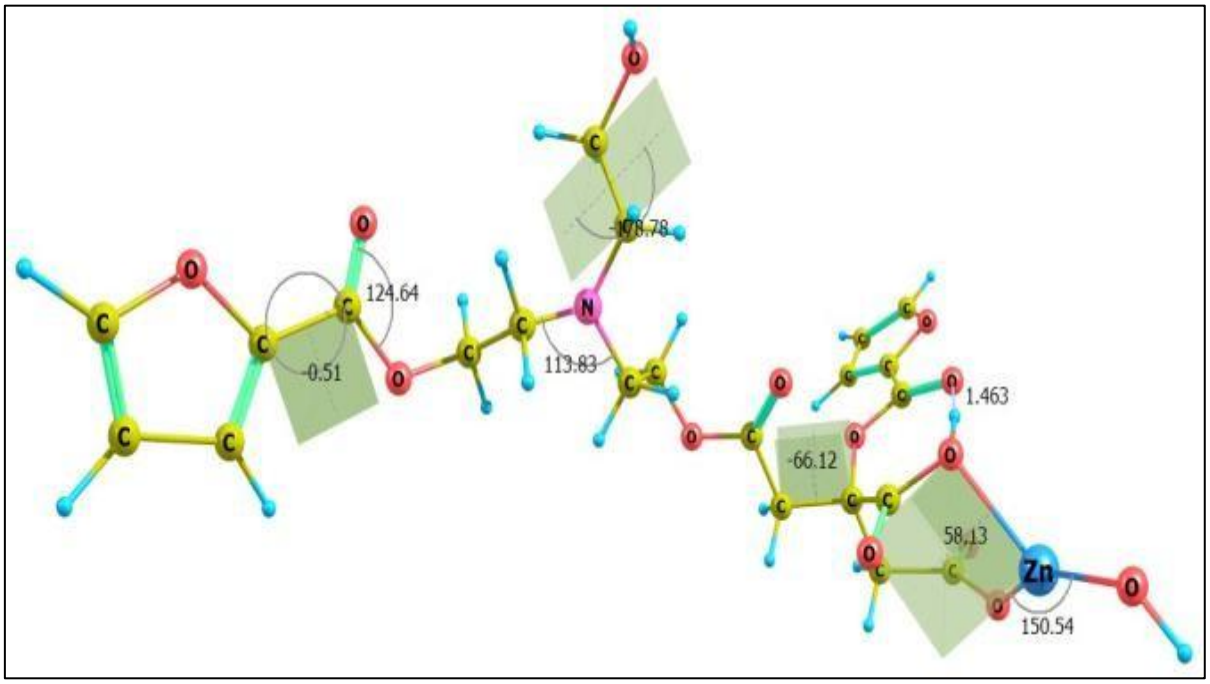

Fig. 14 : The Optimized geometry of the CA_4-ZnO nanocomposite hydrogels

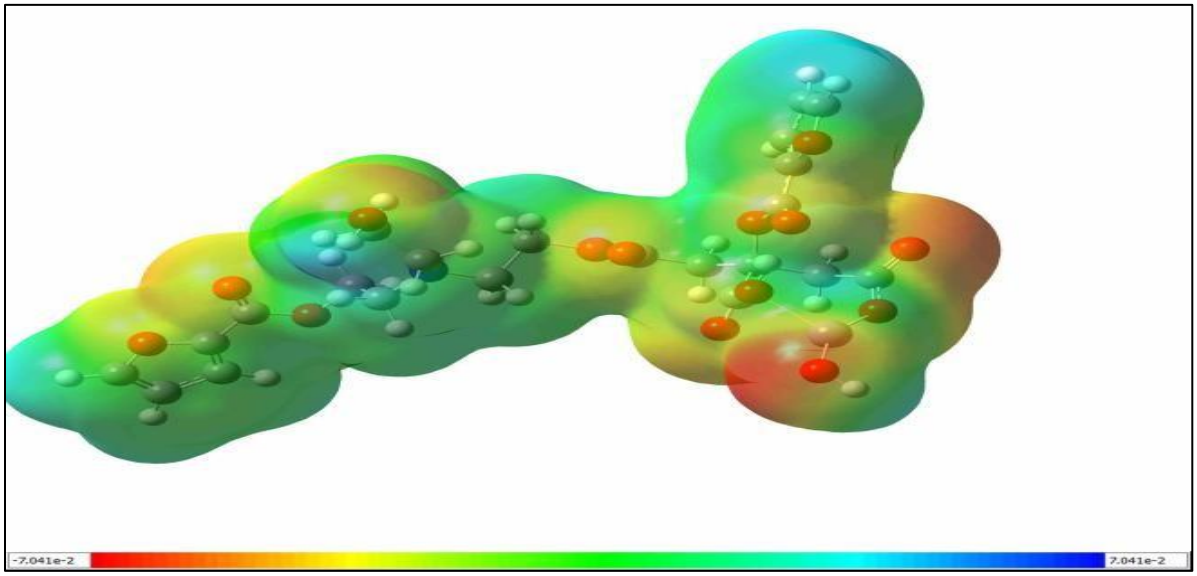

Fig. 15 :The MESP of the CA_4-ZnO nanocomposite hydrogels

3.3.2 Molecular Docking (pdb id:1N67 and 4DXD)

In view of the biomedical properties, nanocomposite hydrogels were identified for docking studies against important receptors involved in healing anti-bacterial infections, FtsZ (Filamenting temperature-sensitive mutant Z) in protein complex [35] and biomedical targets involving *Staphylococcus aureus* proteins: Clumping Factor A [36] Infections caused by drug-resistant strains of *Klebsiella pneumoniae* pose the major threat to the efficacy of conventional antibiotics. Therefore, there is an increasing need to investigate the alternate antimicrobial therapies, especially hydrogels synthesized from simple monomeric compounds [37]. Considering the biological importance of hydrogel derivatives, the present study aimed to synthesize, characterize, and investigate its biological potency of the hydrogel using simple, convenient, and ecofriendly synthetic methodology.

The molecular docking study was evaluated for the interactions of CA_4-ZnO nanocomposite hydrogels as it had good antibacterial property and it involved FtsZ in the protein complex with PDB ID: 4DXD, and CA_4-MgO nanocomposite hydrogels with *Staphylococcus aureus* proteins: *Clumping Factor A* (PDB ID: 1N67) that showed great anti-bacterial property. Both the nanocomposite hydrogels showed favorable docking scores. However, CA_4-ZnO nanocomposite hydrogels with the latter protein showed a stronger and more favorable binding to Clumping Factor A as shown in **Table 6**. CA_4-ZnO nanocomposite hydrogels also demonstrated superior ligand efficiency across all evaluated metrics, including standard (–0.188), surface area-adjusted (–0.633), and log-normalized values (–1.543).

In the CA_4- ZnO Clumping Factor A complex, the ligand is tightly anchored via hydrogen bonds with polar residues (ASN267, SER268, GLN235), and stabilized by hydrophobic contacts (VAL270, VAL323, ALA269, ILE232) and potential electrostatic interactions with ASP273.

Water-mediated interactions and minimal solvent exposure further enhance binding stability. These findings suggest CA_4- ZnO nanocomposite hydrogels may serve as a more effective modulator of *S. aureus* proteins.

Table. 6: The properties and clumping factor A for CA_4-ZnO nanocomposite hydrogels

Property	**Clumping Factor A From Staphylococcus Aureus (1N67) CA_4-ZnO**
Docking Score	-7.154
Glide Ligand Efficiency	-0.188
Glide Ligand Efficiency SA	-0.633
Glide Ligand Efficiency LN	-1.543
Glide G Score	-7.154
Glide Evdw	-21.263
Glide Ecoul	-21.754
Glide Emodel	-42.555
Glide Energy	-43.017
XP GScore	-7.154
XP HBond	-1.860

3.3.3 ADMET (Absorption, Distribution, Metabolism, Excretion, and Toxicity)

The water solubility of a compound (LogS) represents the solubility of the compound at 25 °C . Drug with higher water solubility are absorbed more efficiently than lipid- soluble compounds, and the obtained value of -2.99indicates favorable solubility in aqueous media. Similarly,

intestinal absorption predicts the percentage of orally administered drug. The low absorption value in this study suggests that the compound have more effectively administered through alternative routes rather than oral delivery.

The blood-brain barrier (BBB) indicates the ability of a drug to penetrate into the brain and is an important factor in minimizing side effects and toxicity with enhancing the drug efficacy. The evaluated nanocomposite hydrogels was predicted to readily cross the BBB as presented in **Table. 7**. The obtained value suggests favorable BBB permeability for the investigated drug system.

Table. 7: The properties and BBB ranges for CA_4-ZnO nanocomposite hydrogels

Properties	CA_4-ZnO
Molecular Weight	592.82
Water Solub	-2.99
Caco2 perm	-0.23
Intest Abs	32.4
Skin Perm	-2.73
Glycopro substrate	Yes
BBB Perm	-2.43
CNS Perm	-3.85
CYP1A inhibitor	No
Log P	0.624
Surface area	223.12

4 CONCLUSIONS

In the current research, pH-responsive CA_4 hydrogels with variable nano ZnO concentrations were developed. The UV analysis of the [CA_4-ZnO] complex polymeric hydrogel reveals a strong peak at 300 nm, demonstrating the presence of nano ZnO particles. The FTIR spectroscopy reveals the peak at 1073 cm^{-1} and 1041 cm^{-1} shows the C-O-C stretching frequency. The peak appeared at 670 cm^{-1} which confirms the incorporation of zinc oxide nanoparticles in the main chain of hydrogels. The SEM-EDX of [CA_4- ZnO] reveals heterogeneous, non-porous, with rough surface structure due to hydrogel matrix packed with ZnO nanoparticles, which are scattered irregularly and EDX spectrum has respective amount of C, O, N, and Zn with 56.16, 30.69, 3.29 and 7.51 %, respectively. The TEM analysis of [CA_4-ZnO] nanocomposite hydrogels reveals the 38nm in size. The TGA study reveals that the ZnO nanocomposite hydrogel has considerable thermal stability, with several degradation stages that include water loss, polymer decomposition. The swelling outcomes of hydrogel were also tested at varying pH 2.0-11.0, and they shown that swelling and swelling equilibrium were higher in neutral (pH 7) medium. The swelling studies clearly demonstrate the citric acid has the ability to tune the swelling behavior. The increased concentration of nano ZnO (CA_4Z_3) results in a higher swelling ratio than other hydrogel compounds. Antibacterial investigation of [CA_4-ZnO] nanocomposite hydrogels shows moderate inhibitory zone with the *S. aureus, B. subtilis* and *K. pneumonia*, where as *E. coli* exhibites no antibacterial activity because of difference in its cell membrane permeability towards the antibacterial agent. Similarly, antifungal activity has low zone of inhibition because of the tough chitinous membranes of cells and melanin pigments found in *Aspergillus niger* and *Candida albicans,* making them resistant to oxidative stress and ZnO nanoparticles attack. The antioxidant activity shows that CA_4Z_3 hydrogels have significant antioxidant properties, in higher

concentration of 100, 250 and 500 µg/ml. The average cell viability in cytotoxic assays was greater than 80 % in all concentrations which is good and safe to use in biomedical applications. The docking studies reveals nanocomposite hydrogels can serve as a more effective modulator of *S. aureus* proteins and be readily cross the blood-brain barrier (BBB). As a result, the study concludes that the produced biocompatible pH sensitive hydrogels have promising uses in industrial and biological applications like tissue engineering, wound healing drug delivery and other high performances.

List of Abbreviations

LIST OF ABBREVIATIONS	
CA	Citric acid
TEA	Triethanolamine
FA	2 Furoic acid
CT	Citric acid –Triethanolamine
CTF	Citric acid–Triethanolamine-2 Furoic acid
ZnO	Zinc oxide
FT-IR	Fourier Transform Infrared Spectroscopy
SEM	Scanning Electron Microscopy
TGA	Thermal Gravimetric Analysis
HR-TEM	High-Resolution Transmission Electron Microscopy
UV	Ultraviolet Spectroscopy
EDX	Energy Dispersive X-ray
DPPH	2,2-Diphenyl-1-picrylhydrazyl

MTT	3-(4,5-dimethylthiazol-2-yl)-2,5diphenyltetrazoliumBromide
DMSO	Dimethyl sulfoxide
FMO	Fragment Molecular Orbital
MO	Molecular Orbital
HOMO	Highest Occupied Molecular Orbital
LUMO	Lowest Unoccupied Molecular Orbital
MESP	Molecular Electro Static Potential
IRC	Intrinsic reaction coordinate
BBB	Blood-brain barrier
DFT	Density functional theory
FtsZ	Filamenting temperature-sensitive mutant Z
ADMET	Absorption, Distribution, Metabolism, Excretion and Toxicity
GLN235	Glutamine at position 235
ASN267	Asparagine at position 267
VAL270	Valine at position 270
VAL323	Valine at position 323
ALA269	Alanine at position 269
ILE232	Isoleucine at position232
BHI	Brain Heart Infusion
CFU	Colony-Forming Units
DMEM	Dulbecco's Modified Eagle Medium
PBS	Phosphate- Buffered Saline
LogS	logarithmic value of the aqueous solubility of the compound
SER268	Serine at position 268

ASP273	Aspartic acid at position 273

CONFLICTS OF INTEREST:
Authors declares the no conflicts of interest regarding this manuscript.

AVAILABILITY OF DATA AND MATERIALS:
Data supporting the results of this study are available upon request from the corresponding author.

FUNDING:
No external funding was received for this research.

AI Disclosure:
The authors confirm that no part of the scientific content, data analysis, results, interpretations, or conclusions of the manuscript were generated by artificial intelligence (AI). Grammarly and QuillBot were used solely to improve grammar, language quality, sentence structure, and overall readability of the manuscript. The authors reviewed and verified all revisions made by these tools and take full responsibility for the accuracy, integrity, and originality of the manuscript content, in accordance with COPE guidelines and the journal's AI-use policy.

AUTHOR CONTRIBUTION:
Conceptualization and methodology: R. Princy Sowmya, S. Guhanathan; Investigation and data curation: R. Princy Sowmya, S. Guhanathan.; Formal analysis and validation: S. Guhanathan.; Software and computational studies (DFT and molecular docking): Imran Predhanekar and Attar Kubaib.; Writing—original draft preparation R. Princy Sowmya.; Writing—review and editing: R. Princy Sowmya, S. Nikila and S. Harini.; Visualization: R. Princy Sowmya, S. Nikila and S. Harini.; Supervision and project administration: S. Guhanathan.; All authors have read and agreed to the published version of the manuscript.

ORCID'S

- Princy Sowmya R: 0009-0008-8230-1339
- Nikila S: 0009-0002-9337-1814
- Harini S: 0009-0008-9903-6949
- Kubaib Attar: 0000-0003-0909-0391
- Imran Predhanekar M; 0000-0002-5556-4116
- Prof. Dr. Guhanathan Selvam: 0000-0002-8986-1637

Acknowledgement:
The authors are grateful to Muthurangam Government Arts College for providing the necessary research facilities to carry out this study.

REFERENCES

1. Dodda, J. M., Deshmukh, K., Bezuidenhout, D., &Yeh, Y.-C. (2023). Hydrogels: Definition, History, Classifications, Formation, Constitutive Characteristics, and Applications. In *Multicomponent Hydrogels. The Royal Society of Chemistry *1–25.

2. Bashir, S., Hina, M., Iqbal, J., Rajpar, A. H., Mujtaba, M. A., Alghamdi, N. A., Wageh, S., Ramesh, K., & Ramesh, S. (2020). Fundamental Concepts of Hydrogels: Synthesis, Properties, and Their Applications. *Polymers, 12*(11), 2702.

3. Dhara (Ganguly), M. (2024). Polymer hydrogels: Classification and recent advances. *Journal of Macromolecular Science, Part A*, *61*(5), 265–288.

4. Zhang, K., Liu, Y., Shi, X., Zhang, R., He, Y., Zhang, H., & Wang, W. (2023). Application of polyvinyl alcohol/chitosan copolymer hydrogels in biomedicine: A review. *International Journal of Biological Macromolecules*, *242*, 125192.

5. De Piano, R., Caccavo, D., Barba, A. A., & Lamberti, G. (2024). Swelling Behavior of Anionic Hydrogels: Experiments and Modeling. Gels, 10(12), 813.

6. Zhang, Y.; Wu, B.M (**2023)**. Current Advances in Stimuli-Responsive Hydrogels as Smart Drug Delivery Carriers. *Gels* , *9*, 838.

7. Calderon Moreno, J. M., Chelu, M., &Popa, M. (2025). Biocompatible Stimuli-Sensitive Natural Hydrogels: Recent Advances in Biomedical Applications. *Gels*, *11*(12), 993.

8. Ren, Z.; Ke, T.; Ling, Q.; Zhao, L.; Gu, H (**2021**). Rapid self-healing and self-adhesive chitosan-based hydrogels by host-guest interaction and dynamic covalent bond as flexible sensor. *Carbohydr. Polym.* , *273*, 118533.

9. Nicodemus, G. D., & Bryant, S. J. (2008). Cell Encapsulation in Biodegradable Hydrogels for Tissue Engineering Applications. *Tissue Engineering Part B: Reviews, 14*(2), 149–165.

10. Chamkouri, H. (2021). A Review of Hydrogels, Their Properties and Applications in Medicine. *American Journal of Biomedical Science & Research, 11*(6), 485–493.

11. Rafael, D., Melendres, M. M. R., Andrade, F., Montero, S., Martinez-Trucharte, F., Vilar Hernandez, M., Durán-Lara, E. F., Schwartz Jr, S., &Abasolo, I. (2021). Thermo-responsive hydrogels for cancer local therapy: Challenges and state-of-art. *International Journal of Pharmaceutics, 606*, 120954.

12. Danole, A. B., Kothali, B. K., Apte, A. K., Kulkarni, A. A., Khot, V. S., Patil, A. A., &Upadhye, S. S. (2019). A Review on Hydrogel. *American Journal of PharmTech Research, 9*(1), 71–81.

13. Wang, H., Du, J., & Mao, Y. (2025). Hydrogel-Based Continuum Soft Robots. *Gels*, *11*(4), 254.

14. Mishra, S., Rani, P., Sen, G., &Dey, K. P. (2018). Preparation, properties and application of hydrogels: a review. *Hydrogels: recent advances *, 145-173.

15. Yadav, A., Rajhans, K. P., Ramteke, S., Sahu, B. L., Patel, K. S., &Blazhev, B. (2016). Contamination of Industrial Waste Water in Central India. *Journal of Environmental Protection, 07*(01), 72–81.

16. Ghatti, V., Chapi, S., Kumar Kumarswamy, Y., Nandihalli, N., & Kasai, D. R. (2025). Strontium-Decorated Ag2O Nanoparticles Obtained via Green Synthesis/Polyvinyl Alcohol Films for Wound Dressing Applications. *Materials*, *18*(15), 3568.

17. Pattadakal, S., Ghatti, V., Chapi, S., G., V., Kumarswamy, Y. K., Raghu, M. S., T., V. G., Nandihalli, N., & Kasai, D. R. (2025). Poly(vinyl alcohol) Nanocomposites Reinforced with CuO Nanoparticles Extracted by Ocimum sanctum: Evaluation of Wound-Healing Applications. *Polymers*, *17*(3), 400.

18. Kaushik, M., Niranjan, R., Thangam, R., Madhan, B., Pandiyarasan, V., Ramachandran, C., Oh, D.-H., & Venkatasubbu, G. D. (2019). Investigations on the antimicrobial activity and wound healing potential of ZnO nanoparticles. *Applied Surface Science*, *479*, 1169–1177.

19. R. Princy Sowmya, S. Harini, S. Nikila , S.Guhanathan (2025). Investigation on Effect of 3-Trimethoxysilyl Propyl Methacrylate based Nano-ZnO/CTF Nanocomposite Hydrogel-Synthesis and Characterization. *NanoNEXT*, *6*(1), 1–11.

20. Sakthivel, M., Franklin, D. S., & Guhanathan, S. (2016). pH-sensitiveItaconic acid based polymeric hydrogels for dye removal applications. *Ecotoxicology and Environmental Safety, 134 *, 427–432.

21. Chitra G. , Franklin D.S. , Sudarsan S. , Sakthivel M., Guhanathan S. (2017). Indole-3-acetic acid/diol based pH-sensitive biological macromolecule for antibacterial, antifungal and antioxidant applications. International Journal of Biological Macromolecules, 95, 363–375.

22. Helmiyati, H., Hidayat, Z. S. Z., Sitanggang, I. F. R., & Liftyawati, D. (2021). Antimicrobial packaging of ZnO–Nps infused into CMC–PVA nanocomposite films effectively enhances the physicochemical properties. *Polymer Testing, 104*, 107412.

23. Hamrayev, H., & Shameli, K. (2021). Biopolymer-Based Green Synthesis of Zinc Oxide (ZnO) Nanoparticles. IOP Conference Series:*Materials Science and Engineering, 1051*(1), 012088.

24. Mazaheri, N., naghsh, nooshin, Karimi, A., &Salavati, H. (2019a). In vivo Toxicity Investigation of Magnesium Oxide Nanoparticles in Rat for Environmental and Biomedical Applications. Iranian Journal of Biotechnology, 17(1), 1–9.

25. Sheng, L., Su, L., & Zhang, H. (2015). Experimental determination on thermal parameters of prismatic lithium ion battery cells. International Journal of Heat and Mass Transfer, 139, 231 239.

26. Guhanathan, S., Devi, M. S., & Murugesan, V. (2001). Effect of coupling agents on the mechanical properties of fly ash/polyester particulate composites. Journal of Applied Polymer Science, 82(7),

27. Pourmadadi, M., Rahmani, E., Shamsabadipour, A., Mahtabian, S., Ahmadi, M., Rahdar, A., &Díez-Pascual, A. M. (2022). Role of Iron Oxide (Fe2O3) Nanocomposites in Advanced Biomedical Applications: A State-of-the-Art Review. *Nanomaterials*, *12*(21), 3873. https://doi.org/10.3390/nano12213873

28 Wang, L., Riediger, L., Rao, Q., Xu, X., Nie, Y., Zhou, Y., Zhang, J., Tang, P., Wang, W., Tacke, F., Guillot, A., Vallier, L., Talon, I., Li, W., Yang, Y., Haag, R., & Ma, N. (2026). Tunable Synthetic Hydrogel Modulates Hepatic Lineage Specification of Human Liver Organoid. *Advanced Functional Materials*, *36*(7).

29. Leus, I. v., &Zgurskaya, H. I. (2025). No two are alike: on the role of Klebsiellapneumoniae permeability barriers in antibiotic susceptibility and persistence. *Antimicrobial Agents and Chemotherapy.

30. Azevedo, M. M., Teixeira-Santos, R., Silva, A. P., Cruz, L., Ricardo, E., Pina-Vaz, C., & Rodrigues, A. G. (2015). The effect of antibacterial and non-antibacterial compounds alone or associated with antifugals upon fungi. *Frontiers in Microbiology, 6*,669.

31. S, Nikila., S, Harini., R. PrincySowmya,., Attar Kubaib,., Imran Predhanekar,., & S, Guhanathan. (2025). Synthesis and computational assessment of citric acid and 1,4butanediol based pH sensitive hydrogel networks for cationic dye adsorption. *Discover Chemistry*, *2*(1), 350.

32. Hu, Z., Zhao, R., Wang, F., Ren, L., Wang, L., & Jiang, L. (2026). Stimuli-Responsive Hydrogels in Food Sector: Multi-Component Design, Stimulus-Response Mechanisms, and Broad Applications. *Gels*, *12*(3), 233.

33. Harini S., NikilaS, PrincySowmya R,., Somasundaram.D,,&Guhanathan S. (2026). Eco-friendly polyester hydrogel from almond gum/citric acid/ PVA for efficient removal of grenoble green dye. *Polymers from Renewable Resources*.

34. Patel, A. M., Patel, R. G., & Patel, M. P. (2011). Super absorbent hydrogel based on poly [acrylamide/maleic acid/2-methacryloxy ethyl trimethylammonium chloride]: synthesis, characterization and their application in the removal of chromium (VI) from aqueous solution. *Journal of Macromolecular Science, Part A, 48*(5), 339-347.

35. Mustapha, A., AlSharksi, A., Eze, U., Samaila, R., Ukwah, B., Anyiam, A., Samarasinghe, S., & Ibrahim, M. (2024). Phytochemical Composition, In Silico Molecular Docking Analysis and Antibacterial Activity of Lawsonia inermis Linn Leaves Extracts against Extended Spectrum Beta-Lactamases-Producing Strains of Klebsiella pneumoniae. BioMed, 4(3), 277–292.

36. Nguyen, Q. V., Huynh, D. P., Park, J. H., & Lee, D. S. (2015). Injectable polymeric hydrogels for the delivery of therapeutic agents: A review. *European Polymer Journal, 72*, 602–619.

37. Ahmed, S., Rafi, U. M., Senthil Kumar, R., Bhat, A. R., Berredjem, M., Niranjan, V., C., L., & Rahiman, A. K. (2024). Theoretical, antioxidant, antidiabetic and in silico molecular docking and pharmacokinetics studies of heteroleptic oxovanadium(IV) complexes of thiosemicarbazone based ligands and diclofenac. Journal of Biomolecular Structure and Dynamics, 42(16), 8407 8426.